A model for pH coupling of the SARS-CoV-2 spike protein open/closed equilibrium.

Jim Warwicker

School of Biological Sciences, Faculty of Biology, Medicine and Health, Manchester Institute of Biotechnology, University of Manchester, M1 7DN, UK.

Corresponding author

Jim Warwicker, email jim.warwicker@manchester.ac.uk, tel. +44 (0)161 306 4490

Abstract

SARS-CoV-2, causative agent of the COVID-19 pandemic, is thought to release its RNA genome at either the cell surface or within endosomes, the balance being dependent on spike protein stability, and the complement of receptors, co-receptors and proteases. To investigate possible mediators of pH-dependence, pKa calculations have been made on a set of structures for spike protein ectodomain and fragments from SARS-CoV-2 and other coronaviruses. Dominating a heat map of the aggregated predictions, 3 histidine residues in S2 are consistently predicted as destabilising in pre-fusion (all 3) and post-fusion (2 of 3) structures. Other predicted features include the more moderate energetics of surface salt-bridge interactions, and sidechain-mainchain interactions. Two aspartic acid residues in partially buried salt-bridges have pKas that are calculated to be elevated and destabilising. Notably, the degree of destabilisation is predicted to vary between open and closed receptor binding domain conformations. It is therefore suggested that these groups contribute to a pH-dependence of the open/closed equilibrium. These observations are discussed in the context of SARS-CoV-2 infection, mutagenesis studies, and other human coronaviruses.

Key words

SARS-CoV-2, spike protein, pH-dependence, protein electrostatics, virus entry, coronaviruses

Introduction

Viruses must deliver their genome to the host cell, and for membrane enveloped viruses this occurs either at the cell surface, and fusion with the plasma membrane, or through fusion with an intracellular membrane, subsequent to import into the cell. Influenza is the most well-characterised system, both in terms of the cell and structural biology of infection, and reliance on the endosomal entry pathway [1]. Coronaviruses are membrane enveloped viruses that deliver their RNA genome either through fusion at the plasma or endosomal membranes [2]. Factors that determine which fusion route dominates for a particular virus include cell-surface receptor and availability (dependent on cell type), co-receptors, spike (S) protein structural stability, and which proteases carry out the S1/S2 and S2' cleavages [3]. For SARS-CoV-2, causative agent of the world-wide COVID-19 pandemic, cell surface ACE2 is the primary receptor [4], a novel protease specificity has evolved [5], and the primary route of infection (although this depends on protease location and other factors) may be endosomal [6]. Considering also the export secretory pathway for newly assembled viruses, it is clear that environmental pH is likely to play a part in the infection process. The primary focus for molecular response to pH is the coronavirus spike protein, with analogy to the role of influenza hemagglutinin, where pH-dependent conformational changes underpin endosome-mediated infection [1].

Spike glycoprotein structures for SARS-CoV-2 are accumulating rapidly, mostly in two broad categories, cryo-electron microscopy (cryo-EM) analyses of the S glycoprotein soluble ectodomain (S protein for brevity), and X-ray crystallographic structures of fragments, largely the receptor binding domain (RBD) [7, 8]. In both categories, structures may be S protein alone (normally as a trimer in studies of full length protein) or in complex with receptor (ACE2) or antibody fragments. Two large-scale structural themes are apparent. First, pre-fusion, the RBD populates open (up) or closed (down) conformations, with the open form competent for ACE2 binding. Second, comparison of pre-fusion (S1 and S2) and post-fusion (S2 only) structures reveals not only the absence of the shed S1 protein, but also the large conformational change that uncovers the putative fusion peptide, moving it towards the

anticipated location of the target cellular membrane [9]. A report of S trimer structures at acidic pH, including calorimetric data, leads to the suggestion that a pH-dependent switch biases towards an open conformation at pH 5.5 (around endosomal pH), and a closed conformation at pH 4.0 [10]. It is suggested that this plays a role in avoiding immune surveillance of RBD open forms of the S protein, and also that D614 is a part of the switch. This is an intriguing hypothesis in the context of the establishment of the D614G mutation in SARS-CoV-2 genomes over the first year of the pandemic, and reports that the mutation may either bias towards the (ACE2 binding) open form [11] or act in altering barriers to conformational change between open and closed [12]. Biophysical and thermodynamic data for SARS-CoV-2 S protein are accumulating more slowly than the structural database. Deep mutational scanning of the effect that amino acid substitutions make on RBD expression and ACE2 binding has been performed in a yeast display system [13]. This study is targeted at informing which regions are likely to be more evolutionary restricted, for vaccine design, but it is also valuable for assessing the structural and functional importance of residues for which computational work provides predictions.

Protein regions that mediate biological pH-dependence can be predicted with pKa calculations [14]. Continuum electrostatics has been widely used [15], and constant-pH molecular dynamics allows the explicit inclusion of conformational variation into predictions [16], particularly where a structural focus has already been established. SARS-CoV-2 full length S protein is large (1273 amino acids), locations of sites that may determine pH-dependence have not been determined in detail, and there are an increasing number of cryo-EM structures covering various extents of open and closed conformations in the trimer, at resolutions typically around 3 to 4 Å. In this scenario, a reasonable strategy is to apply continuum electrostatics calculations over the available structures and seek consensus results as the basis for prediction. The algorithm used for this study has been reported previously [17], as has a web implementation of a reduced version [18] that benchmarked the method against known pH-determinants for influenza hemagglutinin. That study also identified two histidine residues predicted to be buried and destabilised in both pre-fusion and post-fusion

SARS-CoV-2 S protein. Reported currently is an extensive study over the rapidly expanding dataset of S protein structures. Averaging reveals features that are consistently reported to stabilise or destabilise the S trimer. Residue D614 does not appear to consistently make strong charge interactions in the dataset, so that the D614G mutation may alter stability through other means. Two salt-bridges (one in the RBD and one in the N-terminal domain, NTD), within each of which an aspartic acid is buried, are predicted to contribute pH-dependence at mild acidic pH. For the more prominent of these two, RBD residue D398, interactions differ between open and closed forms, leading to a prediction of pH-dependence for the open/closed equilibrium.

Results and discussion

Predicted electrostatic frustration in the S protein

The set of 24 SARS-CoV-2 S trimer cryo-EM structures (72 monomers) was assembled from the PDB/RCSB [7] in August 2020. An offline version of the code in use at www.protein-sol.manchester.ac.uk/pka [18] was used to predict pKas, with each S trimer covered in a single calculation. Predicted pKas were assembled into a heat map, split according to S1 and S2 pre-fusion proteins and S2 in the post-fusion form, and sorted according to up and down (RBD) monomer instances. Additionally, pKas were averaged for open and closed monomers and displayed in the same colour-coded format as the web application. Thus, red denotes destabilisation (electrostatic frustration in the fold) and blue stabilisation, in both heat map (Figure 1) and molecular view (Figure 2).

Most obvious in Figures 1 and 2 are three histidines in S2 of the pre-fusion protein, two of which (H1048 and H1064) are conserved in coronaviruses and were reported previously [18]. Histidines 1048 and 1064 are buried in both pre- and post-fusion S2, in a subdomain that adopts the same fold in pre- and post-fusion structures [9]. It was suggested that the electrostatic frustration exhibited by these residues would be relieved if the subdomain transiently unfolded during the transition to post-fusion S2 [18]. A third histidine in S2 (H1088) is also destabilised consistently in the pre-fusion structure, but is present only in SARS-CoV-

2, of the 10 aligned sequences (Figure 1), and is not buried or destabilised to the same extent in the post-fusion structure (6xra) [9]. Histidine 1088 is predicted to contribute to stabilisation of the post-fusion protein relative to the pre-fusion protein at acidic pH values, such as endosomal pH, where histidine would normally be ionised.

There are no other ionisable groups in the trimer dataset predicted to possess the extent and consistent destabilisation of the 3 buried histidines already noted. Rather, there is a mix of groups in differing environments, including partially buried charge pairs, charge-dipole interactions, and charge pairs at monomer-monomer interfaces and surfaces, examples of which are noted in Figure 1, and discussed here. Amongst these are the charge pairs E1031 - R1039 and D1041 - K1045, of which the former is relatively conserved amongst coronaviruses and the latter less so. These charge interactions are partially buried, and thus relatively strong, and in both pre-fusion and post-fusion structures are adjacent to monomer-monomer interfaces, in the same domain as the buried H1048 and H1064.

Considering amino acids not close to the buried histidines, D985 is an interesting case, positioned to act as an N-terminal helix cap in a region that has been engineered to incorporate a stabilising double proline substitution [19]. The 985 position is conserved as either aspartic or glutamic acid in coronaviruses, consistent with it being an important site for spike protein stability. Aspartic acid 294 is another N-terminal helix cap, leading to consistent predicted stabilisation, although it is not conserved across coronaviruses. Several charge pairs exist, with partial burial leading to increased interactions relative to purely solvent exposed location, but generally predicted to be stabilising, including R34 - E191, R328 - D578, D442 - R509, and K773 - D775. Residues E819 and R905 are each partially buried and form interactions with mainchain and sidechain hydrogen bonding groups, which are calculated to be stabilising in some monomers and destabilising in others. Key residue D614 in S1 neighbours K854 of S2, but the interactions for both of these are relatively weak and not consistent with a large influence of loss of charge on the properties of the D614G mutant.

The primary focus of this study is those groups that are predicted to be frustrated in S protein trimers, leading to pKa changes and the potential for pH-dependent effects. From

Figure 2, this filter greatly narrows the ionisable groups of most interest. They are the buried histidines in S2, and two charge pairs in S1.

Partially buried pair D398 - R355 is predicted to couple with the open/closed equilibrium

The two charge pairs that feature predicted electrostatic frustration, when averaged over the dataset, are R355 - D398 in the RBD, and R273 - D290 in the NTD (Figure 2). Focussing on R355 - D398, the aspartic acid has very little solvent accessibility in all structures studied, whilst the arginine burial varies according to structure (Figure 3). Average calculated D398 pKa for closed form monomers is 5.8, and for open form monomers 7.1, with 10 of 11 open monomer pKas at 7.0 or above, and the remaining one slightly lower than the intrinsic pKa of 4.0. In contrast, predicted D398 pKas for the closed form monomers vary across a range of stabilising and destabilising values. The environment of R355 changes between open and closed forms, forming a larger interface with the NTD of a neighbouring monomer in the closed form (Figure 3), but also with variation in the closed interfaces. Indeed, for the 58 instances of RBDs in the closed conformation, R355 solvent accessibility correlates with D398 pKa ($r=0.55$, $p<0.00001$). Average values for D398 pKas in open and closed monomers (Figure 2) are thus the result of (mostly) large-scale destabilisation in the open form, and a conformation-dependent sliding scale of stabilisation/destabilisation in the closed form. Variation of predicted D398 pKas for closed monomers results from modulation of the strong electrostatic coupling between ionised D398 and R355 sidechains (which balances the D398 burial penalty). In closed conformations, more interfacial coverage of R355 leads to greater coupling of ionised D398 and R355, greater counteracting of D398 dehydration and lower, more stabilising, predicted D398 pKa values. The consequence of these calculations is a predicted contribution that destabilises the open form relative to closed from, with a pH-dependence that depends on D398 pKa.

In order to test the calculations for cryo-EM structures, a set of X-ray crystal coordinate sets was assembled for the RBD of SARS-CoV-2 (crystallised alone or in complex with ACE2 or antibody fragments). Since these RBD structures are not within the context of the S trimer,

they represent open conformations. The average predicted D398 pKa for the 10 RBD structures is 7.1, all substantially destabilising, with the lowest at 5.8 (6m0j chain E), in agreement with the cryo-EM structure calculations.

Crystal structures are available for RBDs of 4 of the 7 human coronaviruses (SARS-CoV-1, SARS-CoV-2, MERS, HCoV-HKU1), and a cryo-EM structure for the closed conformer of HCoV-OC43. For the remaining two human CoVs, HCoV-NL63 and HCoV-229E, D398 and R355 (SARS-CoV-2 numbering) are not present in the alignment (Figure 4). A characteristic of the charge couple in open monomer SARS-CoV-2 calculations is that ionised R355 is stabilised and ionised D398 destabilised. This is also evident for predictions in the RBDs of SARS-CoV-1 and MERS, but not for HKU1 or HuOC43 (Figure 4). The collapse of charge coupling between residues equivalent to D398 and R355, and the consequent loss of pH-dependence, for HKU1 and HuOC43 are due to sequence and structure changes in this region. In HKU1 the residue equivalent to Y396 is valine, and in HuOC43 it is threonine, the smaller sidechains increasing solvent accessibility at the site corresponding to R355. The residue equivalent to F464 is glycine in HKU1, and this region of HuOC43 folds away from the charge couple, the effect in both HKU1 and HuOC43 being to reduce the solvent accessibility of residues equivalent to both R355 and D398. Thus, pH-dependent differential stabilisation of open and closed trimers is predicted for the severe human infections, SARS-CoV-1, SARS-CoV-2, and MERS, but not for the other 4 known human coronaviruses, HKU1, HuOC43, NL63, 229E.

Charge pair R273 - D290 in the NTD is qualitatively similar to R355 - D398, with D290 having very low solvent accessibility and R273 greater solvent accessibility. Interpreting open versus closed is not as straightforward for the NTD, since the NTD most affected by an open monomer (RBD up) will be one of the other two monomers in the trimer. Thus, NTDs were re-assigned as open or closed according to the relevant contact RBD, giving an average predicted D290 pKa of 3.9 for 12 NTDs neighbouring an open RBD, and 5.5 for 57 other NTDs in the trimer dataset. However, a correlation between arginine solvent accessibility and aspartic acid pKa, that is observed for R355 - D398, is not seen here. Given this lack of

correlation and the lower predicted D290 pKas, compared with D398, the R273 - D290 pair is not pursued further in this report.

Environment of the D398 - R355 charge pair

A number of reports impact on the prediction that R355 - D398 contributes to a pH-dependence of the open/closed equilibrium, with more open forms being increasingly disfavoured as pH rises through the mild acidic range. Notably, a pH-dependent switch has been suggested for the open/closed equilibrium [10]. Further, it is suggested that the D614G mutation partially destabilises this switch. Interestingly, pKa calculations with the current trimer dataset give no indication that D614 has sufficiently strong interactions to generate a substantial pH-dependence. An outstanding issue is the balance of structural effects caused by D614G mutation, including loss of D614 mediated interactions and destabilisation of the closed trimer with increased ACE2 binding potential [11], and the mutation G614 facilitating increased interactions [12]. Indeed, it is reported that the effect of the D614G mutation is to order a region that forms a wedge and stabilises monomer packing within the trimer [12]. This packing suggestion is reminiscent of the effect of fatty acid binding, evident in trimer structures, stabilising interactions in the closed form [20]. The fatty acid binding region is in a subdomain of the RBD that lies adjacent to the R355 - D398 pair, and which consistently in crystal structures has higher B-factors than the subdomain responsible for ACE2 binding (Figure 3). If the flexibility of this region is dependent on fatty acid binding, then it could couple to alteration of R355 solvent accessibility and thus, according to the current work, D398 pKa and pH-dependent conformational biasing of closed versus open conformation.

In a series of structures of furin cleaved S trimers [21], most of which were released after collation of the trimer dataset, predicted D398 pKas for one extreme (6zgi, all monomers down) are all stabilising, those for all monomers open (7a98, 3 ACE2 bound) are all destabilising. Intermediate combinations of open/closed monomers within a trimer are predicted to have mixed (stabilising, destabilising) pKas. These results, for a set of trimer structures from the same laboratory, that vary from entirely closed to entirely open, are in

agreement with calculations for the original trimer dataset, with the consequence being a predicted pH-dependence of the open/closed equilibrium.

Analysis of the effects of mutation to the full set of amino acid alternatives, at RBD locations, recapitulates the divide between RBD subdomains located proximal and distal to the ACE2 binding region [13]. Greater tolerance of mutations is observed, with respect to both ACE2 binding and RBD expression, in the distal subdomain, consistent with the higher B-factors seen in crystal structures. Both R355 and D398, which lie at a junction between these subdomains, are uniquely favoured for expression, and largely favoured for ACE2 binding [13]. This is not surprising if the coupling between R355 and D398 is important for stability. Although D398 is predicted to be destabilised in many of the structures, this is more than compensated by predicted stabilisation of R355, due to the pair interaction. It is interesting that for F464, which occludes both R355 and D398, the two mutations that are tolerated for expression are tyrosine and glycine. Tyrosine is presumably a swap for similar, whereas glycine would increase solvent accessibility around the charge pair and reduce the coupling, as suggested for the RBD of HKU1. In circulating SARS-CoV-2 genomes, mutations of R355, D398, (or F464), are not currently accumulating [22], in line with a functional role. Residue Y423 is positioned to accept or donate in hydrogen bond interaction with D398, so that the buried environment of D398 appears to be compatible with either ionised or protonated sidechain. Tyrosine 423 is also a key residue in the scanning mutation analysis [13].

Cold sensitivity of a spike protein construct is reduced when the protein is engineered to bias towards the closed/down trimer [23]. It is also significantly reduced when the pH is reduced from 7.4 to 6.0, although the molecular origin of this pH effect, and thus whether the R355 - D398 charge pair is involved, is unknown. The scope for a functional role of pH in the viral infection cycle is apparent at multiple points, demonstrated for example in a study of interferon stimulated genes in viral replication [24] that includes endosomal (pH 6.5 to 5.5), and secretory pathway (pH 7 to 5) candidates. It has been reported that evolution of the furin cleavage site at the S1/S2 junction and the D614G mutation act to balance infectivity and

stability of SARS-CoV-2 [25]. The current work suggests that the R355 - D398 pair could be another factor in this balance, including a pH-dependent element.

Conclusions

The expanding dataset of SARS-CoV-2 S protein trimers and fragments has been leveraged to yield pKa predictions that focus on a small number of amino acids, when interrogated for those that show electrostatic frustration. Prominent amongst these is the partially buried salt bridge D398 - R355 in the RBD, which is predicted to contribute a stability difference between open and closed forms, due to opposing burial (destabilising) and charge pair interaction (stabilising) terms that are summarised in Figure 5. Variation with pH is also predicted, of potential relevance to virus cell entry and exit. The importance of charge coupling between R355 and D398 could be examined with double mutation, simultaneously replacing both ionisable groups.

Materials and methods

Structural datasets

A set of 24 S trimers for SARS-CoV-2 was created from the August 2020 RCSB/PDB, with the S proteins extracted from complexes where necessary: 6vsb, 6vxx, 6vyb, 6xkl, 6z43, 6xm5, 6x6p, 6x29, 6x2c, 6x2a, 7byr, 6zge, 6zgg, 6xcm, 6xs6, 6zp1, 6zp0, 6zoy, 6xr8, 6zox, 6xlu, 6xm4, 6xm3, 6xm0. These are all cryo-EM structures, with resolutions mostly in the range 3 – 4 Å.

The RCSB was searched for X-ray crystallographic structures of coronavirus RBD and NTD, with a specific subset collated for SARS-CoV-2 data, in September 2020. These X-ray structures are generally higher resolution than the S trimer cryo-EM structures. Retrieved data for SARS-CoV-2 RBD (PDB and chain) were 6lzgB, 6mojE, 6w41C, 6ylaA, 6yz5E, 6z2mA, 6zczA, 7bwjE, 7c8vB, and chain E of the chimeric 6vw1 structure. For structures of RBDs obtained from human coronaviruses other than SARS-CoV-2, single representatives were taken: 2ghvE (SARS-CoV-1), 4kqzA (MERS), 5kwbA (HKU1), and 6nzkA (HuOC43), where

6nzkA is a cryo-EM structure in the closed form and the others are X-ray crystal structures. A dataset of NTD representative structures was also collected for coronaviruses that infect humans, 6x29A (SARS-CoV-2), 5x4sA (SARS-CoV-1), 5x4rA (MERS), 6nzkA (HuOC43), 5i08C (HKU1). Of these, 6x29, 6nzk, and 5i08 are cryo-EM structures.

Sequence datasets

In order to visualise amino acid sequence conservation alongside electrostatics calculations, a set of 10 S protein sequences was collected, covering the coronavirus family, with UniProt [26] identifiers and coronavirus sub-family: P0DTC2 (SARS-CoV-2, beta), P59594 (SARS-CoV-1, beta), K9N5Q8 (MERS, beta), A3EXG6 (Bat-HKU9, beta), P11224 (MHV-A59, beta), P11223 (Avian-IBV, gamma), Q91AV1 (Porcine-EDV, alpha), P15423 (Human-229E, alpha), P10033 (Feline-IPV, alpha), and B6VDW0 (Bulbul-HKU11, delta). Sequences were aligned with Clustal Omega [27] at the European Bioinformatics Institute [28], and visualised in ESPript [29]. A conservation score was calculated from the number of occurrences of each SARS-CoV-2 amino acid in the alignment of 10 sequences, colour-coded for display (Figure 1).

Electrostatics calculations

A model for combined Finite Difference Poisson Boltzmann (FDPB) and Debye-Hückel (DH) continuum electrostatics calculations, termed FD/DH, has been introduced and benchmarked [17]. A feature of this model is the ability to discriminate between largely buried ionisable groups, that may individually contribute substantially to folded state stabilisation or destabilisation (the latter termed here electrostatic frustration), and those groups that are solvent accessible and typically contribute less. The latter includes most salt-bridge interactions, which are folded-state stabilising and are normally plentiful across a protein surface. Recently a web tool has been reported (www.protein-sol.manchester.ac.uk/pka) [18], that allows users to visualise predictions of ionisable group pKas around specified centres, with the FD/DH method. In the current work, an offline version of the method is used to make pKa predictions for Asp, Glu, Lys, Arg, and His groups for submitted structures, without the

requirement for centre and subset specification of the rapid turnaround web tool. Calculations are made for 24 SARS-CoV-2 S trimers, with results visualised as a heat map of predicted pKa deviations, colour-coded as for the web tool, and presented in columns of aligned groups. Where the S protein numbering differs from that of the base structure (6vsb), a register correction is made to maintain the 6vsb numbering scheme. Average predicted ΔpKa is calculated for each ionisable group and placed into a structure file for comparable visualisation (using PyMOL) to that of the web tool (red destabilising, blue stabilising).

Key Points

- Application of pKa calculations across the rapidly increasing dataset of SARS-CoV-2 spike protein trimers and fragments yields a set of consensus predictions that focus on a small number of amino acids.
- A partially buried salt bridge (D398 – R355) in the receptor binding domain is predicted to contribute a stability difference between open and closed forms, which varies in the mild acidic pH region, of relevance to cell entry of the virus and its secretion.
- The salt-bridge lies at a nexus of protein flexibility, is present in SARS-CoV-2, SARS-CoV-1 and MERS, but either absent or predicted to be less influential in other human coronaviruses.
- A strategy of simultaneous mutation for D398 and R355, and characterisation, would probe the charge pair role in SARS-CoV-2 infectivity.

Funding

This work was support by the UK Engineering and Physical Sciences Research Council (grant number EP/N024796/1).

Acknowledgements

Staff of the University of Manchester Computational Shared facility are thanked for technical support.

Conflict of interest

There are no conflicts of interest to declare.

Data availability statement

The data underlying this article will be shared on reasonable request to the corresponding author.

References

1. Benton DJ, Gamblin SJ, Rosenthal PB, *et al.* Structural transitions in influenza haemagglutinin at membrane fusion pH. *Nature* 2020;**583**:150-153.
2. Millet JK, Whittaker GR. Physiological and molecular triggers for SARS-CoV membrane fusion and entry into host cells. *Virology* 2018;**517**:3-8.
3. Kirchdoerfer RN, Wang N, Pallesen J, *et al.* Stabilized coronavirus spikes are resistant to conformational changes induced by receptor recognition or proteolysis. *Sci Rep* 2018;**8**:15701.
4. Yan R, Zhang Y, Li Y, *et al*. Structural basis for the recognition of SARS-CoV-2 by full-length human ACE2. *Science* 2020;**367**:1444-1448.
5. Jaimes JA, Millet JK, Whittaker GR. Proteolytic Cleavage of the SARS-CoV-2 Spike Protein and the Role of the Novel S1/S2 Site. *iScience* 2020;**23**:101212.
6. Morris G, Athan E, Walder K, *et al.* Can endolysosomal deacidification and inhibition of autophagy prevent severe COVID-19? *Life Sciences* 2020;**262**:118541.
7. Berman H, Henrick K, Nakamura H, *et al.* The worldwide Protein Data Bank (wwPDB): ensuring a single, uniform archive of PDB data. *Nucleic Acids Res* 2007;**35**:D301-303.
8. Gowthaman R, Guest JD, Yin R, *et al.* CoV3D: a database of high resolution coronavirus protein structures. *Nucleic Acids Res* 2020, doi: 10.1093/nar/gkaa731.
9. Cai Y, Zhang J, Xiao T, *et al.* Distinct conformational states of SARS-CoV-2 spike protein. *Science* 2020;**369**:1586-1592.
10. Zhou T, Tsybovsky Y, Olia AS, *et al.* A pH-dependent switch mediates conformational masking of SARS-CoV-2 spike. bioRxiv 2020, doi: https://doi.org/10.1101/2020.07.04.187989.
11. Yurkovetskiy L, Wang X, Pascal KE, *et al.* Structural and Functional Analysis of the D614G SARS-CoV-2 Spike Protein Variant. *Cell* 2020, doi: 10.1016/j.cell.2020.09.032.
12. Zhang J, Cai Y, Xiao T, *et al.* Structural impact on SARS-CoV-2 spike protein by D614G substitution. bioRxiv 2020, doi: https://doi.org/10.1101/2020.10.13.337980.
13. Starr TN, Greaney AJ, Hilton SK, *et al.* Deep Mutational Scanning of SARS-CoV-2 Receptor Binding Domain Reveals Constraints on Folding and ACE2 Binding. *Cell* 2020;**182**:1295-1310 e1220.
14. Alexov E, Mehler EL, Baker N, *et al.* Progress in the prediction of pKa values in proteins. *Proteins* 2011;**79**:3260-3275.
15. Gunner MR, Baker NA. Continuum Electrostatics Approaches to Calculating pKas and Ems in Proteins. *Methods in Enzymology* 2016;**578**:1-20.

16. Chen W, Morrow BH, Shi C, *et al.* Recent development and application of constant pH molecular dynamics. *Molecular Simulation* 2014;**40**:830-838.
17. Warwicker J. Improved pKa calculations through flexibility based sampling of a water-dominated interaction scheme. *Protein Sci* 2004;**13**:2793-2805.
18. Hebditch M, Warwicker J. protein-sol pKa: prediction of electrostatic frustration, with application to coronaviruses. *Bioinformatics* 2020, doi: 10.1093/bioinformatics/btaa646.
19. Wrapp D, Wang N, Corbett KS, *et al.* Cryo-EM structure of the 2019-nCoV spike in the prefusion conformation. *Science* 2020;**367**:1260-1263.
20. Toelzer C, Gupta K, Yadav SKN, *et al.* Free fatty acid binding pocket in the locked structure of SARS-CoV-2 spike protein. *Science* 2020, doi: 10.1126/science.abd3255.
21. Benton DJ, Wrobel AG, Xu P, *et al.* Receptor binding and priming of the spike protein of SARS-CoV-2 for membrane fusion. *Nature* 2020, doi: 10.1038/s41586-020-2772-0.
22. Portelli S, Olshansky M, Rodrigues CHM, *et al.* Exploring the structural distribution of genetic variation in SARS-CoV-2 with the COVID-3D online resource. *Nature Genetics* 2020;**52**:999-1001.
23. Edwards RJ, Mansouri K, Stalls V, *et al.* Cold sensitivity of the SARS-CoV-2 spike ectodomain. bioRxiv 2020, doi: https://doi.org/10.1101/2020.07.12.199588.
24. Martin-Sancho L, Lewinski MK, Pache L, *et al.* Functional Landscape of SARS-CoV-2 Cellular Restriction. bioRxiv 2020, doi: https://doi.org/10.1101/2020.09.29.319566.
25. Nguyen HT, Zhang S, Wang Q, *et al.* Spike glycoprotein and host cell determinants of SARS-CoV-2 entry and cytopathic effects. bioRxiv 2020, doi: https://doi.org/10.1101/2020.10.22.351569.
26. UniProt C. UniProt: a worldwide hub of protein knowledge. *Nucleic Acids Res* 2019;**47**:D506-D515.
27. Sievers F, Wilm A, Dineen D, *et al.* Fast, scalable generation of high-quality protein multiple sequence alignments using Clustal Omega. *Mol Syst Biol* 2011;**7**:539.
28. Madeira F, Park YM, Lee J, *et al.* The EMBL-EBI search and sequence analysis tools APIs in 2019. *Nucleic Acids Res* 2019;**47**:W636-W641.
29. Robert X, Gouet P. Deciphering key features in protein structures with the new ENDscript server. *Nucleic Acids Res* 2014;**42**:W320-324.

Figure Legends

Figure 1. Ionisable group properties in the trimer dataset. Predicted changes in ionisable group pKas in a heat map, from brighter red (destabilising) to darker blue (stabilising), with separate panels for S1 (upper) and S2 (lower) proteins. Calculations are grouped according to open and closed monomers (RBD), as indicated. Sequence conservation across coronaviruses is shown with a deeper purple for greater conservation. Residues discussed in the text are listed, and the extent of NTD and RBD domains is displayed for S1.

Figure 2. Averaged predicted ΔpKas in molecular display. Ionisable groups are coloured using the same scale as Figure 1 (red is destabilising, blue is stabilising), here with averages

over the open (A) and closed (B) form monomers. Sites of greater destabilisation are highlighted and their identity noted.

Figure 3. The environment of charge pair R355 - D398 in open and closed forms. A view of R355 - D398 (6lzgB) indicates the extensive burial of D398 and partial burial of R355 (A). The charge pair is represented as magenta spheres in the 6lzgB crystal structure, which is aligned to open (B) and closed (C) monomers in the 6vsb trimer context. Colouring of the RBD crystal structure shows a substantially higher crystal B-factor for a region on one side of the charge pair.

Figure 4. The R355 - D398 pair in human coronaviruses. Predicted destabilising and stabilising ΔpKas of R355 and D398 for the 5 human coronaviruses with available RBD structural information (A). Sequences for the 7 human coronavirus are aligned over this region (B), with secondary structure added from 6vsbB, and sequence conservation displayed (ESPript). Locations of R355 and D398 are indicated with purple spheres.

Figure 5. A delicate balance of predicted charge interactions. Tube representation for closed (6zgi) and open (7a98) S trimers, with the R355 - D398 charge pair denoted in magenta. The qualitative balance between favourable charge coupling (+) and unfavourable burial (-) terms is given, with an estimated net contribution. Thus, in the closed form, large burial and coupling terms for D398 approximately cancel to give a normal pKa, whilst burial outweighs coupling in the open form, giving a destabilising ΔpKa. Combined D398 and R355 terms are estimated to be stabilising for the closed form, but closer to zero for the open form, with the difference (favouring of the closed form) being pH-dependent.

Figure 1

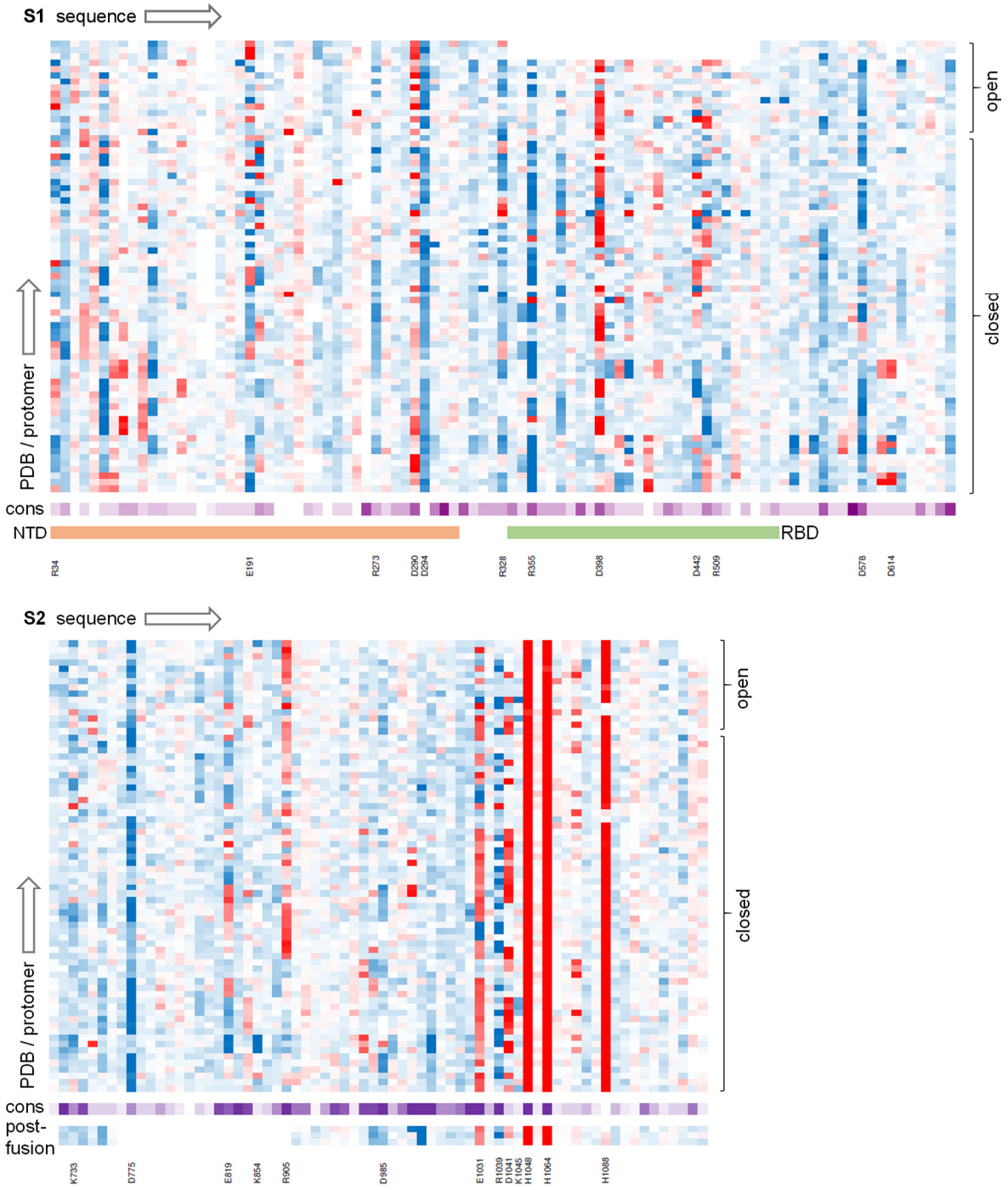
S1 sequence
PDB / protomer
open
closed
cons
NTD
RBD
R34
E191
R273
D290
D294
R328
R355
D398
D442
R509
D578
D614
S2 sequence
PDB / protomer
open
closed
cons
post-
fusion
K733
D775
E819
K854
R905
D985
E1031
R1039
D1041
K1045
H1048
H1064
H1088

Figure 2

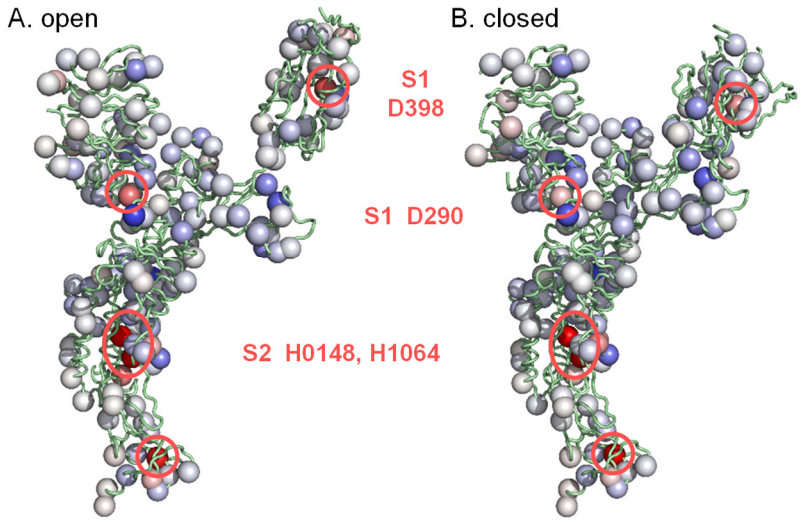

Figure 3

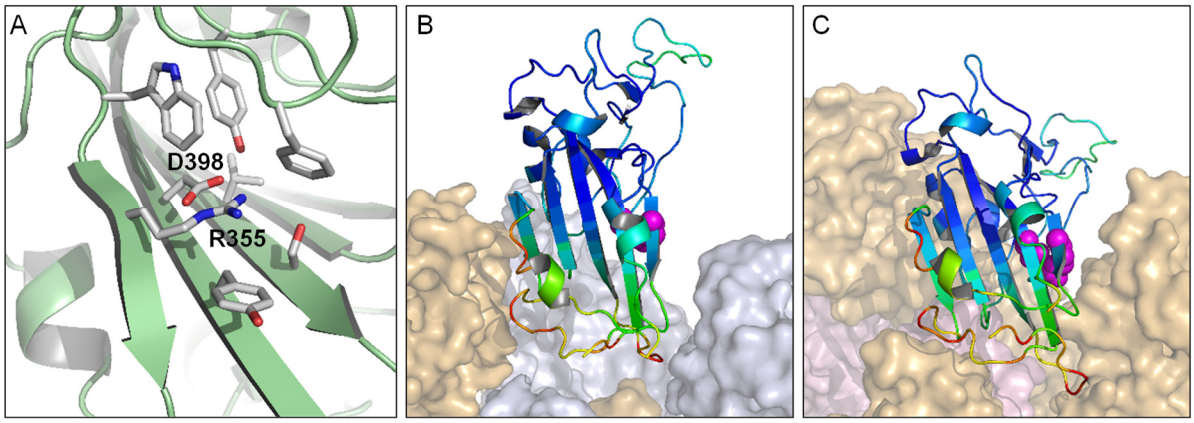

Figure 4

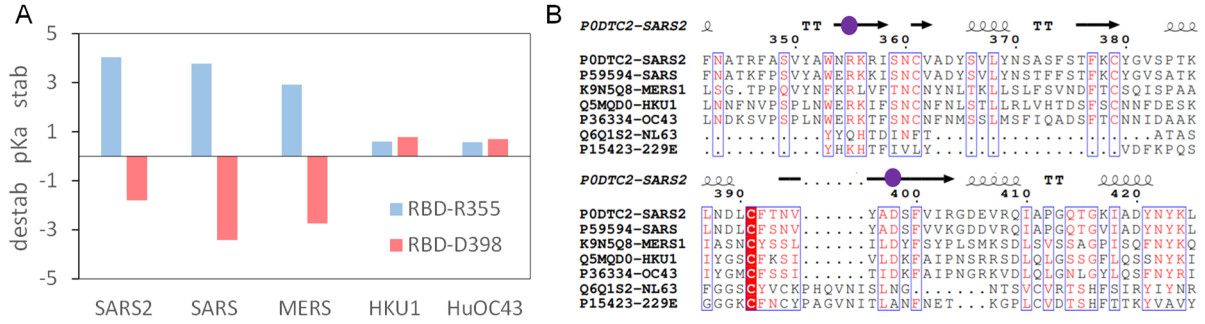
A
destab pKa stab
5
3
1
-1
-3
-5
RBD-R355
RBD-D398
SARS2
SARS
MERS
HKU1
HuOC43
B
P0DTC2-SARS2
350
360
370
380
P0DTC2-SARS2
P59594-SARS
K9N5Q8-MERS1
Q5MQD0-HKU1
P36334-OC43
Q6Q1S2-NL63
P15423-229E
390
400
410
420

Figure 5

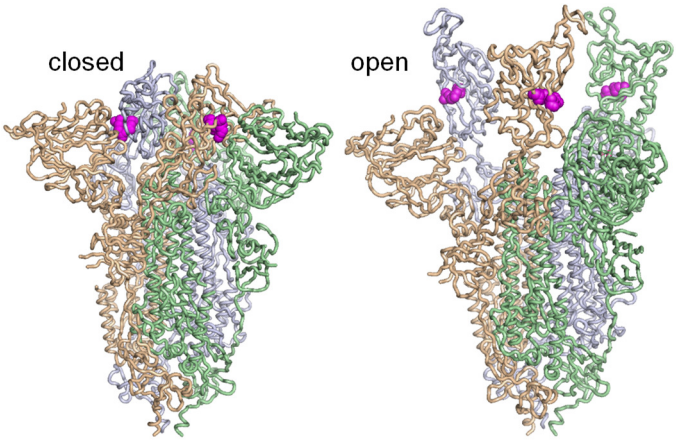

	closed			open		
	burial	couple	net	burial	couple	net
D398	---	+++	0	---	++	-
R355	--	+++	+	-	++	+